An analysis of the hyperfine parameters of the $RFe_{11}Ti$ and $RFe_{11}TiH$ compounds, where R is a rare-earth element

2006 J. Phys.: Condens. Matter 18 205

(http://iopscience.iop.org/0953-8984/18/1/015)

INSTITUTE OF PHYSICS PUBLISHING JOURNAL OF PHYSICS: CONDENSED MATTER

J. Phys.: Condens. Matter **18** (2006) 205–219 doi:10.1088/0953-8984/18/1/015

An analysis of the hyperfine parameters of the $RFe_{11}Ti$ and $RFe_{11}TiH$ compounds, where R is a rare-earth element

Cristina Piquer[1], **Fernande Grandjean**[2], **Olivier Isnard**[3,4] **and Gary J Long**[5]

[1] Instituto de Ciencia de Materiales de Aragón–CSIC, Universidad de Zaragoza, E-50009 Zaragoza, Spain
[2] Department of Physics, B5, University of Liège, B-4000 Sart-Tilman, Belgium
[3] Laboratoire de Cristallographie, CNRS, associé à l'Université J. Fourier, BP 166X, F-38042 Grenoble Cedex, France
[4] Institut Universitaire de France, Maison des Universités, 103 Boulevard Saint-Michel, F-75005 Paris, Cedex, France
[5] Department of Chemistry, University of Missouri-Rolla, Rolla, MO 65409-0010, USA

E-mail: cpiquer@unizar.es, fgrandjean@ulg.ac.be, olivier.isnard@grenoble.cnrs.fr and glong@umr.edu

Received 21 July 2005
Published 9 December 2005
Online at stacks.iop.org/JPhysCM/18/205

Abstract

The Mössbauer spectra of $CeFe_{11}Ti$ and $CeFe_{11}TiH$ obtained between 4.2 and 295 K are analysed in terms of the model used to analyse the spectra of the $RFe_{11}Ti$ and $RFe_{11}TiH$ compounds, where R is Pr, Nd, Sm, Gd, Tb, Dy, Ho, Er and Lu. The hyperfine parameters obtained with a consistent model that considers both the easy magnetization direction and the titanium preferential site occupancy are discussed as a function of rare-earth atomic number, temperature and hydrogen content. The average hyperfine fields in the $RFe_{11}Ti$ and $RFe_{11}TiH$ compounds are described with a two-sublattice model in which the iron sublattice contributions coincide with the fields observed in $LuFe_{11}Ti$ and $LuFe_{11}TiH$, respectively. In both series, the rare-earth sublattice contributes a transferred field which occurs as a result of indirect exchange between the rare-earth 4f and iron 3d electrons and depends on the nature of the rare-earth element. The increase in average hyperfine field and isomer shift upon hydrogenation of the $RFe_{11}Ti$ compounds results from the unit-cell expansion upon hydride formation. The observed average quadrupole shift is closely related to the magnetic anisotropy exhibited by each compound.

1. Introduction

The series of $RFe_{11}Ti$ compounds and their hydrides, $RFe_{11}TiH$, where R is a rare-earth element, all of which crystallize in the $ThMn_{12}$ structure with the $I4/mmm$ space group,

Table 1. Mössbauer spectral hyperfine parameters for $CeFe_{11}Ti$.

Parameter	T (K)	8f	8i	8j	Wt av.
$H_0(\Delta H)$ (T)	295	23.4 (−2.5)	28.9 (−1.7)	24.6 (−2.4)	22.9
	225	25.4 (−2.7)	30.7 (−1.9)	26.8 (−2.7)	24.9
	155	26.9 (−2.8)	32.3 (−1.8)	28.3 (−2.8)	26.4
	85	27.9 (−2.9)	33.4 (−1.9)	29.3 (−2.9)	27.3
	4.2	28.4 (−2.9)	33.8 (−1.9)	29.8 (−2.9)	27.8
$\delta_0^a(\Delta\delta)$ (mm s^{-1})	295	−0.200 (0.035)	−0.007 (−0.008)	−0.140 (−0.006)	−0.118
	225	−0.145 (0.035)	0.044 (−0.008)	−0.080 (−0.006)	−0.062
	155	−0.108 (0.035)	0.081 (−0.008)	−0.035 (−0.006)	−0.022
	85	−0.082 (0.034)	0.104 (−0.004)	0.003 (−0.009)	0.007
	4.2	−0.066 (0.034)	0.114 (−0.004)	0.013 (−0.009)	0.019
$\varepsilon_0(\Delta\varepsilon)$ (mm s^{-1})	295	0.044 (0.056)	0.110 (0.007)	−0.070 (0.082)	0.070
	225	0.063 (0.083)	0.140 (−0.003)	0.000 (0.031)	0.099
	155	0.070 (0.070)	0.081 (0.009)	0.013 (0.013)	0.083
	85	0.113 (0.057)	0.145 (0.009)	0.031 (0.002)	0.115
	4.2	0.107 (0.057)	0.147 (0.009)	0.048 (0.002)	0.119

[a] Relative to room temperature α-iron foil.

are potential candidate permanent magnet materials and exhibit a wide variety of magnetic behaviour. Hence, they are of interest both for technological and fundamental studies.

The authors have systematically studied [1–9] the crystallographic, magnetic and Mössbauer spectral properties of the $RFe_{11}Ti$ and $RFe_{11}TiH$ compounds, where R is Ce, Pr, Nd, Sm, Gd, Tb, Dy, Ho, Er and Lu, between 4.2 and 295 K. Except for $CeFe_{11}Ti$ and $CeFe_{11}TiH$, the Mössbauer spectra have all been analysed with a consistent model that considers both the easy magnetization direction and the distribution of titanium in the near-neighbour environment of the three crystallographically inequivalent iron sites in these compounds. The earlier, different, analysis [1] of the Mössbauer spectra of $CeFe_{11}Ti$ and $CeFe_{11}TiH$ is revised in section 2 of this paper.

From the earlier Mössbauer spectral work [1–9], extensive information has been obtained on the hyperfine parameters of the $RFe_{11}Ti$ and $RFe_{11}TiH$ compounds and, consequently, it is of value to examine their variation as a function of rare-earth element, temperature and hydrogen content; see section 3. A summary of the crystallographic and magnetic properties of these compounds, together with a phenomenological model for the magnetic anisotropy and its temperature dependence is presented in a companion paper [10] to this paper.

2. Mössbauer spectra of $CeFe_{11}Ti$ and $CeFe_{11}TiH$

The Mössbauer spectra of $CeFe_{11}Ti$ and $CeFe_{11}TiH$ obtained between 4.2 and 295 K are shown in figures 1(a) and (b), respectively. The spectra have been analysed with a model [2–9] that considers both the axial easy magnetization direction and the distribution of titanium in the near-neighbour environment of the three crystallographically inequivalent iron sites. Hence, nine sextets are required to satisfactorily fit the spectra. Three sextets with 6.47, 10.79 and 9.58% areas represent the 8i site, whereas three sextets each, with 11.51, 15.34 and 9.38 per cent areas represent the 8f and 8j sites. The fits obtained with this model are very good as is shown in figures 1(a) and (b). The hyperfine parameters for $CeFe_{11}Ti$ and $CeFe_{11}TiH$ are given in tables 1 and 2. The estimated errors are at most ±0.2 T for the hyperfine fields, ±0.01 mm s^{-1} for the isomer shift and ±0.02 mm s^{-1} for the quadrupole shift. The fitted line widths were typically about 0.36 mm s^{-1}.

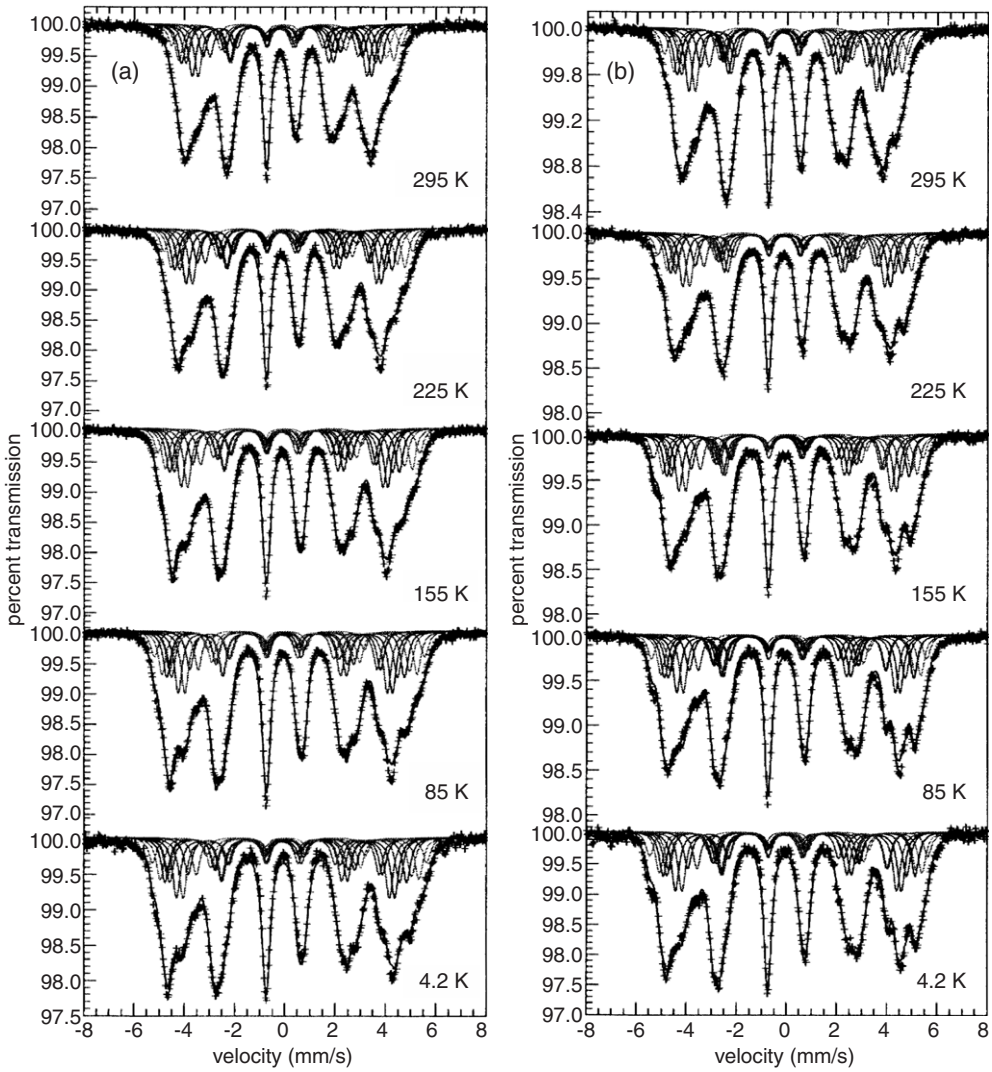

Figure 1. The Mössbauer spectra of $CeFe_{11}Ti$, (a), and $CeFe_{11}TiH$, (b), obtained at the indicated temperatures.

The adequacy of the model is further supported by the temperature dependencies of the hyperfine parameters. The temperature dependence of the maximum hyperfine field, the field measured at an iron which has zero titanium near neighbours, and of their weighted average, in $CeFe_{11}Ti$ and $CeFe_{11}TiH$ is shown in figures 2(a) and (b), respectively. The solid lines are the result of a least-squares fit [11] with the equation

$$B = B_0[1 - C_{3/2}(T/T_C)^{3/2} - C_{5/2}(T/T_C)^{5/2}],$$

where B_0 and T_C are the saturation field and Curie temperature, respectively. Curie temperatures of 487 and 542 K were used [12] for $CeFe_{11}Ti$ and $CeFe_{11}TiH$, respectively. The $C_{3/2}$ and $C_{5/2}$ coefficients are equal to 0.06 ± 0.02 and 0.45 ± 0.10, and 0.15 ± 0.02 and 0.35 ± 0.03, for $CeFe_{11}Ti$ and $CeFe_{11}TiH$, respectively. Similar values have been obtained [2–9] for the other $RFe_{11}Ti$ and $RFe_{11}TiH$ compounds.

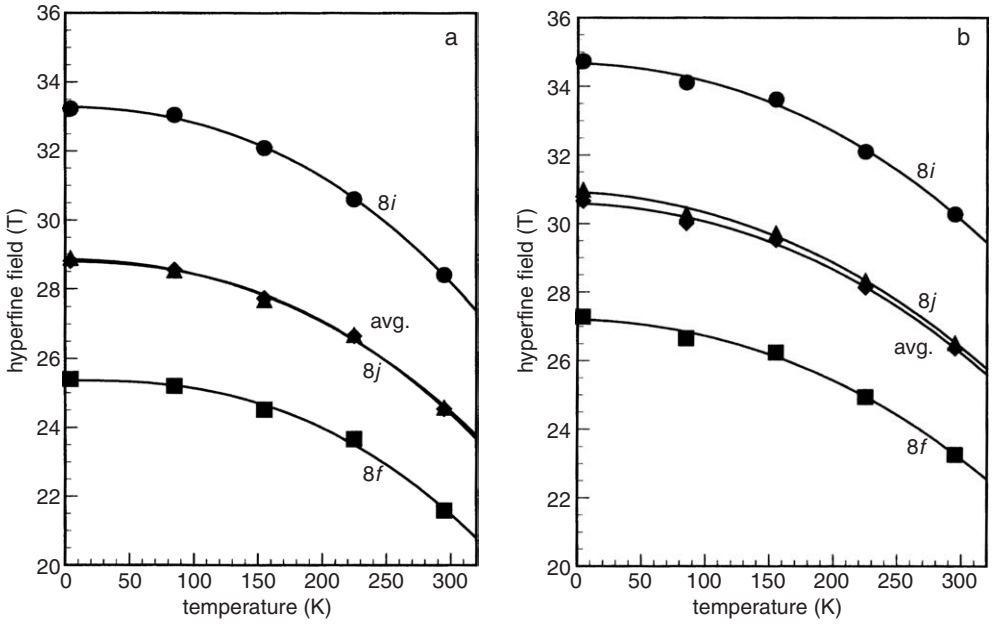

Figure 2. The temperature dependence of the maximum hyperfine field at the three iron sites, and their weighted average, in $CeFe_{11}Ti$, (a), and $CeFe_{11}TiH$, (b). The solid lines are the result of the fit described in the text.

Table 2. Mössbauer spectral hyperfine parameters for $CeFe_{11}TiH$.

Parameter	T (K)	8f	8i	8j	Wt av.
$H_0(\Delta H)$ (T)	295	25.4 (−2.9)	30.1 (−1.9)	26.7 (−2.7)	24.6
	225	27.2 (−3.0)	32.3 (−2.0)	28.7 (−3.0)	26.4
	155	28.5 (−3.0)	33.4 (−1.9)	30.0 (−3.1)	27.7
	85	29.3 (−3.1)	34.1 (−1.9)	30.9 (−3.2)	28.4
	4.2	29.7 (−3.1)	34.4 (−1.9)	31.2 (−3.2)	28.7
$\delta_0^a(\Delta\delta)$ (mm s^{-1})	295	−0.145 (0.024)	−0.064 (0.031)	−0.104 (−0.009)	−0.092
	225	−0.084 (0.027)	0.017 (0.014)	−0.046 (−0.014)	−0.034
	155	−0.051 (0.030)	0.042 (0.023)	0.000 (−0.015)	0.005
	85	−0.016 (0.027)	0.071 (0.031)	0.028 (−0.015)	0.037
	4.2	−0.007 (0.027)	0.076 (0.031)	0.036 (−0.015)	0.045
ε_0 $(\Delta\varepsilon)$ (mm s^{-1})	295	−0.025 (0.114)	0.018 (0.095)	0.020 (0.072)	0.096
	225	−0.014 (0.125)	0.039 (0.073)	0.031 (0.051)	0.100
	155	0.016 (0.128)	0.013 (0.093)	0.061 (0.012)	0.108
	85	0.020 (0.150)	0.031 (0.088)	0.107 (−0.021)	0.126
	4.2	0.027 (0.150)	0.034 (0.088)	0.109 (0.089)	0.130

[a] Relative to room temperature α-iron foil.

The temperature dependence of the site average isomer shift at the three iron sites, and their weighted average, is shown in figures 3(a) and (b) for $CeFe_{11}Ti$ and $CeFe_{11}Ti$ H, respectively. In agreement with the second-order Doppler shift, all isomer shifts decrease with increasing temperature. The fit of the temperature dependence of the weighted average isomer shift with the Debye model yields the expected [13, 14] effective vibrating mass of 57 g mol^{-1} and an effective Mössbauer temperature of 362 and 334 K for $CeFe_{11}Ti$ and $CeFe_{11}TiH$, respectively.

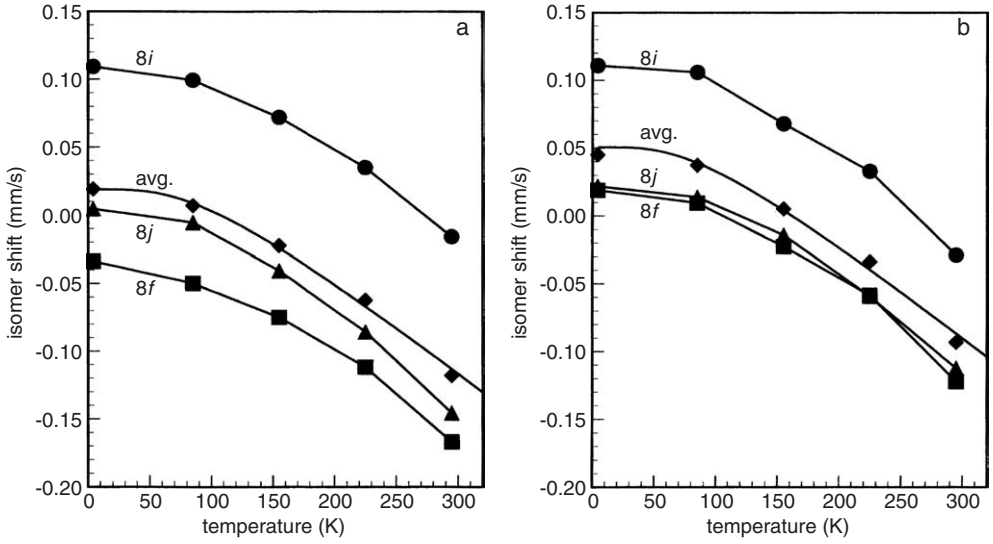

Figure 3. The temperature dependence of the site average isomer shift at the three iron sites, and their weighted average, in $CeFe_{11}Ti$, (a), and $CeFe_{11}TiH$, (b). The solid line for the weighted average isomer shift is the result of a fit with the Debye model for the second-order Doppler shift.

The sequence of isomer shifts, 8i > 8j > 8f, follows the sequence of decreasing Wigner–Seitz cell volumes [15] in both compounds. The increase of 0.03 mm s^{-1} in weighted average isomer shift upon hydrogenation results from the unit-cell expansion of 4 $Å^3$. The increase in the 8f isomer shift is larger than the increases in the 8i and 8j isomer shifts.

3. Analysis of the hyperfine fields

The average hyperfine fields measured at 4.2 and 295 K in $RFe_{11}Ti$ and $RFe_{11}TiH$ as a function of the atomic number of the rare-earth element, R, are shown at the top of figure 4. The trends are slightly different at 4.2 and 295 K, mainly because of the rather low Curie temperature when R is Ce and Lu. At 4.2 K the average hyperfine field increases from Ce to Pr, is nearly constant from Pr to Dy, and decreases from Dy to Lu. The goal of the present study is to determine the origin of this dependence and to identify the mechanisms involved, be they steric, electronic and/or magnetic. In the lower two panels of figure 4, the unit-cell volume and the Curie temperature of the $RFe_{11}Ti$ and $RFe_{11}TiH$ compounds are plotted as a function of the atomic number of the rare-earth element, R. Clearly, the R dependence of the average hyperfine field measured at 4.2 and 295 K and that of the unit-cell volume are quite different. Hence, a steric effect alone cannot explain the observed R dependence of the average hyperfine field. In contrast, the R dependence of the average hyperfine field measured at 295 K and that of the Curie temperature are very similar.

The model developed by Piquer *et al* [16] to analyse the hyperfine fields in the $RFe_{11.5}Ta_{0.5}$ compounds can be applied to analyse the R dependence of the average hyperfine field in the $RFe_{11}Ti$ and $RFe_{11}TiH$ compounds. The hyperfine field at the iron nucleus, in the absence of an external field, can be written as

$$B_{\rm hf}(k) = B_{\rm c} + B_{\rm orb} + B_{\rm dip} = B_{\rm cp} + B_{\rm 4s} + B_{\rm t} + B_{\rm orb} + B_{\rm dip}$$
$$= \alpha\mu_{\rm Fe}(k) + \beta\mu_{\rm Fe}(k) + \zeta_{\rm Fe}(k)Z_{\rm Fe}(k)\langle\mu_{\rm Fe}\rangle_{\rm 1nn} + \zeta_{\rm R}(k)\gamma_{\rm R}n_{\rm RFe}\mu_{\rm R} + B_{\rm anis}. \qquad (1)$$

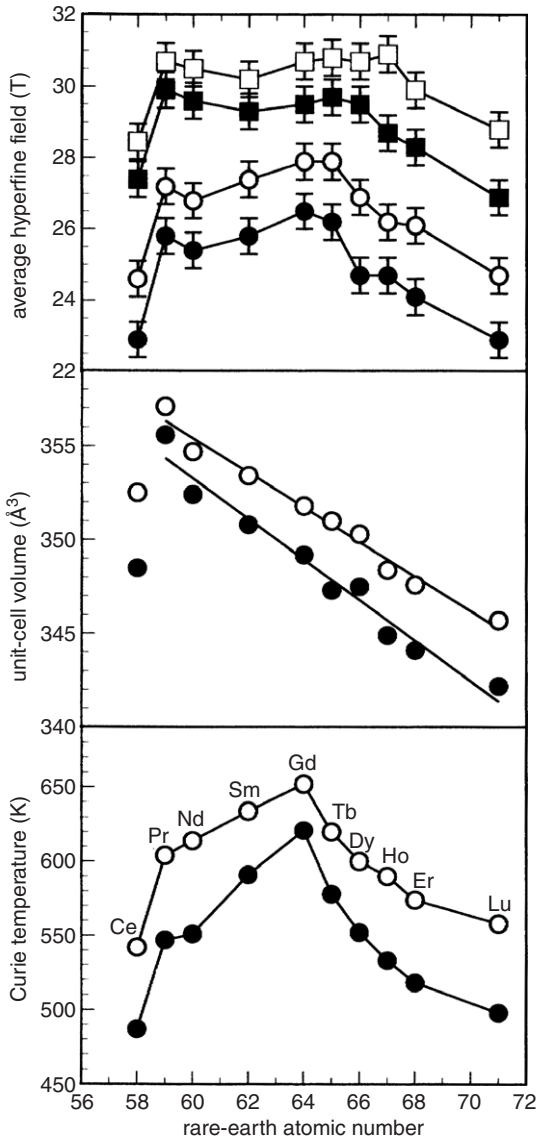

Figure 4. From top to bottom, the 4.2 K, squares, and 295 K, circles, average hyperfine field, the unit-cell volume, and the Curie temperature, in $RFe_{11}Ti$, solid symbols, and $RFe_{11}TiH$, open symbols, as a function of rare-earth atomic number.

The Fermi contact field, B_c, is made up by the sum of three terms, $B_c = B_{cp} + B_{4s} + B_t$. The core polarization term, B_{cp} [17–22], arises from the polarization of the 1s, 2s and 3s core electron spin density by the 3d electrons of the central atom or ion and is proportional to the 3d magnetic moment. So, it can be written as $B_{cp}(k) = \alpha\mu_{Fe}(k)$, where $\mu_{Fe}(k)$ is the local magnetic moment, in μ_B, of the iron at the k site and α, in T/μ_B, is the field at the nucleus produced by a 3d local iron moment of one Bohr magneton, μ_B. The B_{4s} term represents [17, 18] the contribution to the field arising from the polarization of the 4s spin density by the 3d electrons of the central atom or ion. Consequently, for an iron atom or ion

at a given site, k, this term can be written [19, 20] as $B_{4s}(k) = \beta\mu_{Fe}(k)$ where β, in T/μ_B, mainly depends [19] on the number of 4s spins that contribute to the polarization and the magnitude of the 4s–3d intra-atomic exchange interaction. The B_t term is usually referred to as the transferred hyperfine field and represents the contribution arising from the polarization of the 4s spin density by the magnetic moments of the first neighbours, a polarization that occurs because the 4s electrons are much more delocalized than the core electrons. Because the first neighbours may be either iron or rare-earth atoms or ions, this term can be written as the sum of two contributions,

$$B_t = B_{tFe} + B_{tR}. \tag{2}$$

By using a mean field approximation, the iron sublattice transferred field, B_{tFe}, may be assumed to be proportional to the average magnetic moment of the iron in the first-neighbour shell, $\langle\mu_{Fe}\rangle_{1nn}$, and to the number of iron first neighbours, $Z_{Fe}(k)$, with a proportionality factor, $\zeta_{Fe}(k)$, in T/μ_B, that may be different for each iron site, a factor that depends on the number of 4s spins contributing to the polarization, on the intensity of the interatomic 3d–4s exchange interaction and on the particular magnetic and crystallographic environment of the iron site. The rare-earth transferred field, B_{tR}, is assumed to result from the polarization, by the rare-earth 4f electrons, of the rare-earth 5d electrons that are hybridized with the iron 3d electrons. Under this assumption, B_{tR} is proportional to the exchange field acting on the iron,

$$B_{tR} = \zeta_R(k)\gamma_R n_{RFe}\mu_R, \tag{3}$$

where $\gamma_R = 2(g_J - 1)/g_J$, μ_R is the rare-earth magnetic moment, n_{RFe} is the iron–rare-earth exchange coefficient and $\zeta_R(k)$ is a proportionality factor, in T/μ_B, which depends both on the number of 4s spins contributing to the polarization and on the particular magnetic and crystallographic environment of the iron atom or ion. The remaining terms in equation 1 are the dipolar and orbital contributions to the hyperfine field. These contributions are anisotropic, i.e., they depend upon the relative orientation of the magnetization, the magnetic axis and the local principal symmetry axis. For a compound with axial symmetry the dipolar term can be written as $B_{dip} = -2\mu_B\langle S\rangle\langle r^{-3}\rangle\langle 3\cos^2\theta - 1\rangle$, where θ is the angle between the magnetic moment direction and the principal axis of the electric field gradient tensor at a given iron site. The last term, B_{orb}, is the magnetic field at the nucleus resulting from the orbital angular momentum, L, of the unpaired electrons and is given by $B_{orb} = -2\,\mu_B\langle L\rangle\langle r^{-3}\rangle$. For the 3d elements, the crystalline electric field nearly quenches the orbital magnetic moment, but a residual orbital moment may remain and may be related to the spin moment by $\langle L\rangle = (\gamma - 2)\langle S\rangle$, where γ is the Landé electronic factor. The difference in the γ factors for the directions parallel and perpendicular to the principal symmetry axis of a given site gives rise to the anisotropy of the orbital contribution to the field [23]. These two anisotropic contributions, B_{orb} and B_{dip}, are combined into a single contribution, B_{anis} in equation (1).

If the values of $\mu_{Fe}(k)$ are known at different temperatures, the above model can be used [16] to obtain the β and $\zeta_{Fe}(k)$ parameters and the different contributions to $\langle B_{hf}\rangle$. Unfortunately, the values of $\mu_{Fe}(k)$ are not known for the $RFe_{11}Ti$ compounds. However, the model can be used to analyse the origin and the probable contribution of the rare-earth transferred field, B_{tR}. By using the average for the three inequivalent crystallographic iron sites in equation (1), the expression for the total average hyperfine field is

$$\langle B_{hf}\rangle = [\langle\alpha\rangle + \langle\beta\rangle + \langle\zeta_{Fe}\rangle]\langle\mu_{Fe}\rangle + \langle B_{tR}\rangle + \langle B_{anis}\rangle. \tag{4}$$

To a first approximation, the B_{tR} term can be estimated by using a two-sublattice model, i.e., by assuming that, in a magnetic rare-earth compound, the total hyperfine field can be written as

$$\langle B_{hf}\rangle = B_{Fe} + B_{tR}, \tag{5}$$

where B_{Fe} and B_{tR} represent the independent contributions from the iron and rare-earth sublattices, respectively. In the two-sublattice model, the iron sublattice contribution is taken as the experimental value of $\langle B_{hf}\rangle$ of $LuFe_{11}Ti$ and $LuFe_{11}TiH$ for the $RFe_{11}Ti$ and $RFe_{11}TiH$ compounds, respectively, because lutetium is a non-magnetic rare earth.

Some precautions must be taken when applying the two-sublattice model. Specifically, it has been observed [24] that the orbital contribution to the field is different in the axial and canted magnetic phases of $Nd_2Fe_{14}B$. Hence, the orbital and anisotropic contribution to the field in the $RFe_{11}Ti$ and $RFe_{11}TiH$ compounds may also be different in the axial and basal magnetic phases of these compounds; contributions of between 0.1 and 3.7 T are expected. Consequently, within the two-sublattice model, an additional anisotropic contribution, not included in B_{Fe}, may exist but cannot be determined from the experimental results. Moreover, this contribution may be of the same order of magnitude as B_{tR} and its omission may lead to large errors in the determination of B_{tR}. In view of this problem, we believe that the two-sublattice model is only applicable to the axial $RFe_{11}Ti$ and $RFe_{11}TiH$ compounds.

In conclusion, for the axial $RFe_{11}Ti$ and $RFe_{11}TiH$ magnetic compounds, the total magnetic hyperfine field can be written as

$$\langle B_{hf}\rangle = B_{Fe} + \langle\zeta_R\rangle\gamma_R n_{RFe}\mu_R, \tag{6}$$

where B_{Fe} is the iron sublattice contribution, i.e., the average hyperfine field measured for $LuFe_{11}Ti$ or $LuFe_{11}TiH$, respectively.

The 4.2 and 295 K average hyperfine field values in the $RFe_{11}Ti$ compounds are shown in figure 5(a) as a function of the $\gamma_R n_{RFe}\mu_R$ product. An identical plot showing the results for only the axial $RFe_{11}Ti$ compounds is shown in figure 5(b). At 4.2 K $ErFe_{11}Ti$ exhibits a canted magnetic phase with a very small canting angle and it has been assumed to be axial in this figure. Similar plots are shown in figures 6(a) and (b) for the $RFe_{11}TiH$ compounds. In figures 5 and 6, the values of n_{RFe} are obtained from the Curie temperatures and the values of μ_R are the effective rare-earth magnetic moments which are given by $g_J J$. It should be noted that a decrease in the rare-earth magnetic moment has been reported [25] upon hydrogenation of the $RFe_{11}Ti$ compounds.

As is shown in figures 5(b) and 6(b), the average hyperfine fields in the axial compounds vary linearly with the product $\gamma_R n_{RFe}\mu_R$, in agreement with equation (6). Further, the intercept, B_{Fe}, is in good agreement with the measured average hyperfine field in $LuFe_{11}Ti$ and $LuFe_{11}TiH$ both at 4.2 and 295 K. More specifically, the intercepts in figures 5(b) are 27.1 and 23.1 T and the average hyperfine fields in $LuFe_{11}Ti$ are 27.0 and 22.9 T, at 4.2 and 295 K, respectively, whereas the intercepts in figure 6(b) are 28.6 and 24.6 T and the average hyperfine fields in $LuFe_{11}TiH$ are 28.8 and 24.7 T at 4.2 and 295 K, respectively. In figure 5(b), the slopes of the straight line, i.e., the proportionality factor, ζ_R, are 0.021 and 0.029 T/μ_B, at 4.2 and 295 K, respectively, whereas in figure 6(b), the slopes are 0.014 and 0.025 T/μ_B, at 4.2 and 295 K, respectively. The variation in ζ_R in going from the $RFe_{11}Ti$ compounds to the $RFe_{11}TiH$ compounds may result from the change in electronic structure as a consequence of the hydrogen insertion. However, this variation must be interpreted with caution because, if the rare-earth magnetic moment is smaller [25] in the $RFe_{11}TiH$ compounds than in the $RFe_{11}Ti$ compounds, a different larger proportionality factor, ζ_R, will be obtained. For comparison, a value of 0.015 T/μ_B is found [16] in the $RFe_{11.5}Ta_{0.5}$ compounds.

Li *et al* [20] have proposed, on the basis of RKKY interactions, that the rare-earth transferred hyperfine field contribution, B_{tR}, results from the polarization of the 4s iron electrons by the 4f rare-earth moments and, hence, is proportional to $(g_J - 1)J_R$. With this hypothesis, the average hyperfine field can be written as

$$\langle B_{hf}\rangle = B_{Fe} + \langle\zeta_R^{RKKY}\rangle(g_J 1)J_R. \tag{7}$$

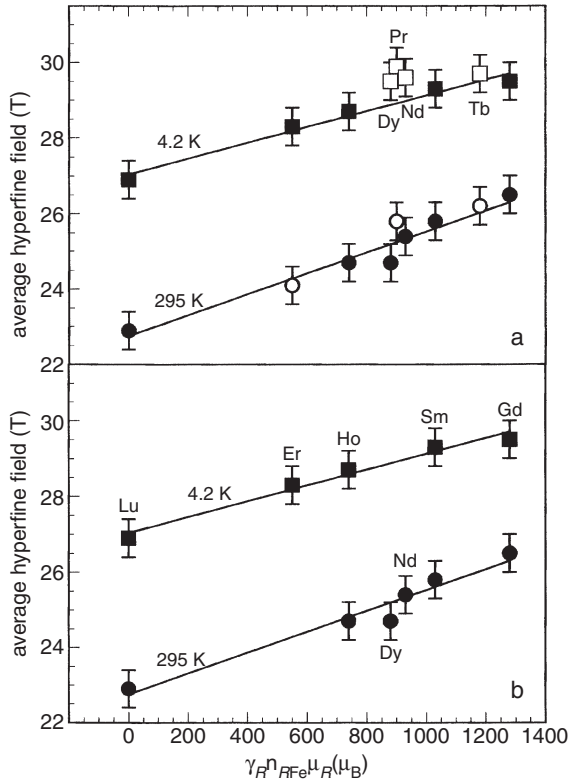

Figure 5. The 4.2 and 295 K average hyperfine field for the $RFe_{11}Ti$ compounds for all R elements, (a), and for the indicated rare-earth elements, (b), as a function of the product $\gamma_R n_{RFe} \mu_R$. The solid and open symbols indicate the axial and planar easy magnetization directions, respectively.

The 4.2 K average hyperfine fields in the $RFe_{11}Ti$ compounds are plotted as a function of the product $(g_J - 1)J_R$ in figure 7(a). In this plot no linear dependence is observed as would be predicted by equation (7). Further, according to equation (7), B_{tR} should have a different sign for the light and heavy rare earths. Hence, the average hyperfine field should be smaller for the light rare-earth compounds, in disagreement with the experimental results. Even if the average hyperfine field is plotted as a function of the modulus of $(g_J 1)J_R$, see figure 7(b), no linear dependence is observed.

The rare-earth dependence of the transferred hyperfine field on a diamagnetic atom or ion in a compound such as a rare-earth phosphide, RP, has been successfully described [26] by considering the rare-earth orbital contribution to the hyperfine field. The application of equation (12) found in [26], with $H_{01} = -1$ T, $H_{10} = 0.08$ T and $H_{21} = 0.5$ T, to the rare-earth dependence of the hyperfine field in the $RFe_{11}Ti$ and $RFe_{11}TiH$ compounds is shown in figure 8. In this figure the observed hyperfine field must be assumed to be negative in order to give the rare-earth dependence of equation (12) for the heavy rare earths. The fit of the experimental data for the heavy rare earths is good but the fit for the light rare earth is very poor. There are several possible reasons for this poor agreement. First, the $RFe_{11}Ti$ and $RFe_{11}TiH$ compounds contain transition metals with 3d electrons, in contrast with the compounds discussed in [26]. Second, in [26], the rare-earth iron exchange parameter, n_{RFe}, was assumed to be constant throughout the rare-earth series, an independence that is not found

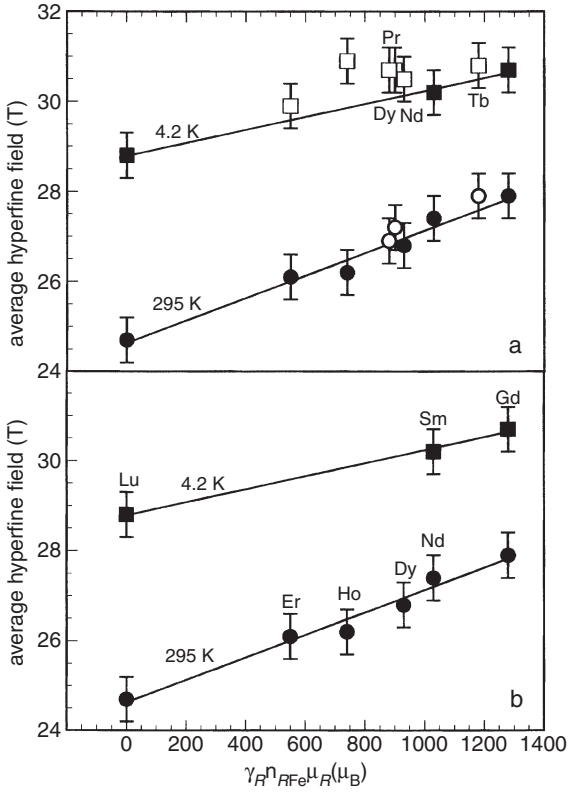

Figure 6. The 4.2 and 295 K average hyperfine field in the $RFe_{11}TiH$ compounds for all R elements, (a), and for the indicated rare-earth elements, (b), as a function of the product $\gamma_R n_{RFe} \mu_R$. The solid and open symbols indicate the axial and planar easy magnetization directions, respectively.

in the $RFe_{11}Ti$ compounds. Finally, the model in [26] predicts different signs for the transferred field from light and heavy rare earths, a change of sign that is not observed in the $RFe_{11}Ti$ compounds.

In conclusion, the rare-earth dependence of the hyperfine field measured at the iron site and hence of the rare-earth transferred field can only be explained by assuming that the rare-earth transferred field results from the polarization of the iron 4s electrons through an indirect mechanism, i.e., polarization by the rare-earth 4f electrons, of the rare-earth 5d electrons that are hybridized with the iron 3d electrons, as has been previously reported [16] for the $RFe_{11.5}Ta_{0.5}$ compounds. This conclusion follows because the hyperfine fields of the light rare-earth members of the $RFe_{11}Ti$ compounds have been measured and cannot be explained either by the model of Li *et al* [20] nor by the orbital contribution to the field [26]. In contrast, the model described herein successfully explains the rare-earth dependence of the hyperfine field in both the $RFe_{11}Ti$ and $RFe_{11}TiH$ compounds and in the $RFe_{11.5}Ta_{0.5}$ compounds [16].

The increase in the 4.2 K average hyperfine field and the expansion in the 295 K unit-cell volume upon hydriding, are shown in figure 9 as a function of rare-earth atomic number. With the exception of terbium, a very good correlation between the increases in the two parameters is observed. Hence, the increase in average hyperfine field upon hydrogenation results essentially from the unit-cell expansion.

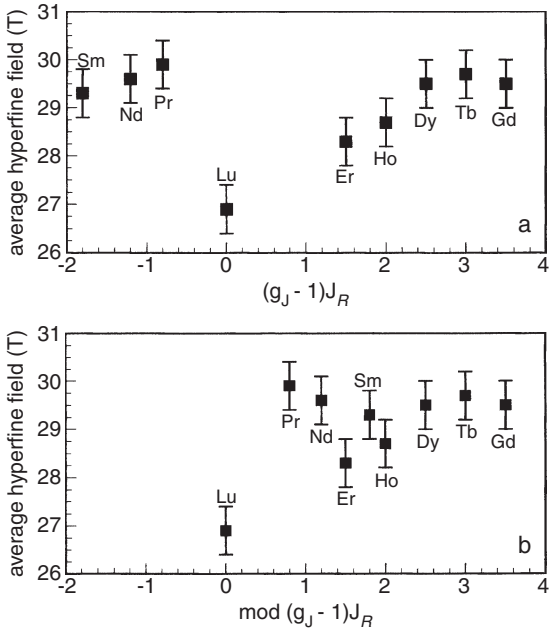

Figure 7. The 4.2 K average hyperfine field in the $RFe_{11}Ti$ compounds as a function of the product, $(g_J - 1)J_R$, (a), and as a function of the product, $|g_J - 1|J_R$, (b).

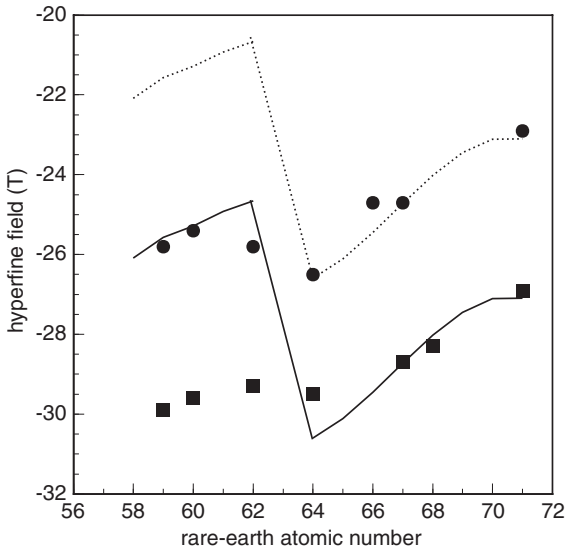

Figure 8. The average hyperfine field in the $RFe_{11}Ti$ compounds as a function of R, obtained at 4.2 K, squares, and 295 K, circles. The solid and dashed curves have been calculated from equation (12) in [26] with the parameters given in the text.

4. Analysis of the isomer shifts

The 4.2 K weighted average isomer shift is shown as a function of rare-earth atomic number for the $RFe_{11}Ti$ and $RFe_{11}TiH$ compounds in figure 10. Within the experimental error limits,

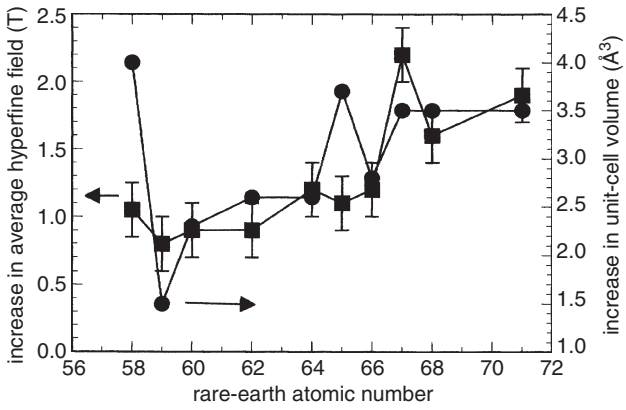

Figure 9. The increase in the 4.2 K average hyperfine field, squares, and 295 K unit-cell volume, circles, upon hydrogenation of the $RFe_{11}Ti$ compounds as a function of the rare-earth atomic number.

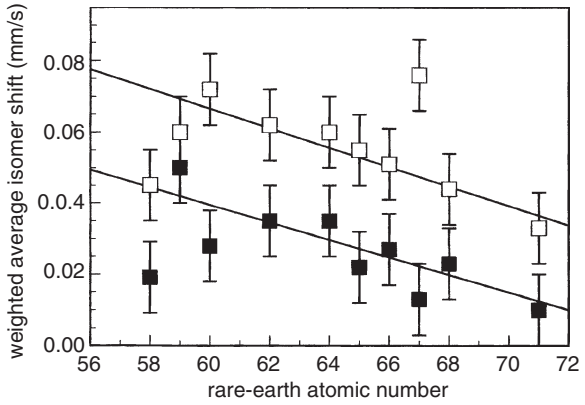

Figure 10. The 4.2 K average isomer shift in the $RFe_{11}Ti$, closed squares, and $RFe_{11}TiH$, open squares, compounds as a function of the rare-earth atomic number. The straight lines are linear fits excluding the Ce and Ho data points.

the average isomer shift decreases from Pr to Lu as expected as a result of the lanthanide contraction. It should be noted that the solid line fits in figure 10 exclude cerium and holmium. Alternatively, a plot of the 4.2 K weighted average isomer shift as a function of the unit-cell volume of the $RFe_{11}Ti$ and $RFe_{11}TiH$ compounds shows a linear behaviour with a slope of 0.002 75 (mm s^{-1}) $Å^{-3}$. The well-known influence of the iron site volume on the isomer shift has been quantified [27] in the past for α-iron as the ratio of the change in isomer shift over the change in the logarithm of the volume. In the $RFe_{11}Ti$ and $RFe_{11}TiH$ compounds, this ratio is 0.89 and 1.00 mm s^{-1}, respectively. These values are only slightly smaller than the value of 1.3 mm s^{-1} reported for α-iron.

The increase in both the weighted average isomer shift and the unit-cell volume, upon hydriding, are shown as a function of rare-earth atomic number in figure 11. With the exception of erbium and lutetium, both increases show similar trends. Hence, the increase in the average isomer shift results mainly from the unit-cell expansion upon hydrogenation.

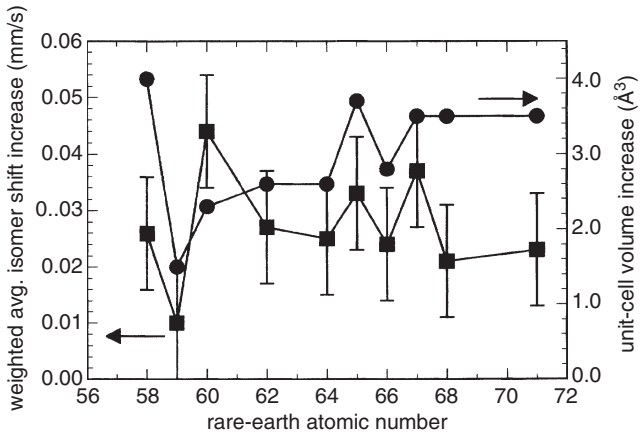

Figure 11. The increase in weighted average isomer shift and unit-cell volume upon hydrogenation of the $RFe_{11}Ti$ compounds as a function of the rare-earth atomic number.

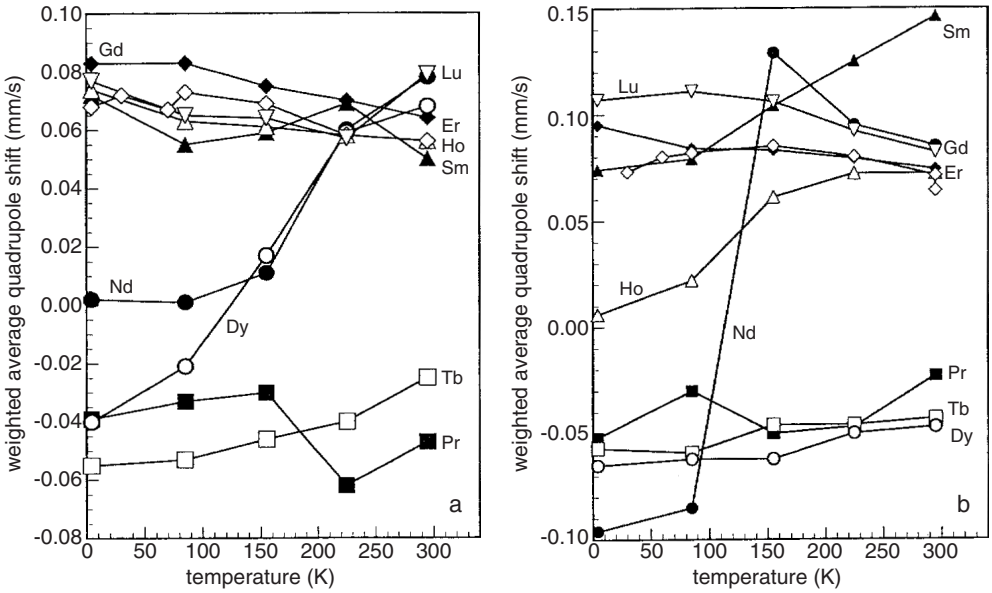

Figure 12. The temperature dependence of the average quadrupole shift in the $RFe_{11}Ti$, (a), and $RFe_{11}TiH$, (b), compounds.

5. Analysis of the quadrupole shifts

The temperature dependence of the average quadrupole shift in the $RFe_{11}Ti$ and $RFe_{11}TiH$ compounds is shown in figures 12(a) and (b), respectively. All the $RFe_{11}TiH$ compounds which undergo a spin-reorientation transition exhibit a change in the average quadrupole shift at the spin-reorientation temperature. Further, all the $RFe_{11}Ti$ and $RFe_{11}TiH$ compounds with an axial easy magnetization direction exhibit a positive average quadrupole shift of about 0.1 mm s^{-1}, whereas compounds with a planar easy magnetization direction exhibit a negative average quadrupole shift of about -0.05 mm s^{-1}. Finally, $HoFe_{11}TiH$, which has a canted

magnetic phase with a relatively large value of the canting angle below its spin-reorientation temperature, exhibits an essentially zero average quadrupole shift.

6. Conclusions

In this paper, we have shown that the average hyperfine field measured in the $RFe_{11}Ti$ and $RFe_{11}TiH$ compounds can be written as a sum of two contributions. The first contribution arises from the iron sublattice and is equal to the average field measured in $LuFe_{11}Ti$ or $LuFe_{11}TiH$. The second contribution is a transferred hyperfine field from the magnetic rare-earth sublattice. This transferred field is proportional to the product $\gamma_R n_{RFe}\mu_R$, where γ_R is $2(g_J - 1)/g_J$, μ_R is the rare-earth magnetic moment, n_{RFe} is the iron–rare-earth exchange coefficient, and μ_R is the rare-earth effective magnetic moment. The proportionality factor, $\zeta_R(k)$, is equal to 0.0021 and 0.0014 T/μ_B at 4.2 K, for the $RFe_{11}Ti$ and $RFe_{11}TiH$ compounds, respectively. This dependence could be established because the hyperfine fields were measured both for the light and heavy rare earths. It indicates that the transferred hyperfine field has its origin in an indirect polarization mechanism of the iron 4s electrons, a mechanism that takes place through the polarization of the iron 3d electrons that are hybridized with the rare-earth 5d electrons, electrons that are themselves polarized by the rare-earth 4f electrons.

The increase in the average hyperfine field and the average isomer shift upon hydrogenation of the $RFe_{11}Ti$ compounds result mainly from the unit-cell expansion. The rare-earth dependence of the average isomer shift reflects the lanthanide contraction. Finally, the average quadrupole shift is closely related to the easy magnetization direction, a positive or negative value indicates an axial or planar easy magnetization direction, respectively, and a close to zero value indicates a large canting angle of the easy magnetization direction.

Acknowledgments

The financial support of the University of Liège for grant number 2850006 and of the 'Fonds de la Recherche Fondamentale Collective' for grant 2.4522.01 is acknowledged with thanks. This work was partially supported by the US National Science Foundation through grants DMR95-21739 and INT-9815138, the Ministère de la Communauté Française de Belgique, convention PVB/ADK/FR/ad2685 and the 'Centre National de la Recherche Scientifique, France' through grants action initiative number 7418.

References

[1] Long G J, Hautot D, Grandjean F, Isnard O and Miraglia S 1999 *J. Magn. Magn. Mater.* **202** 100
[2] Piquer C, Hermann R P, Grandjean F, Long G J and Isnard O 2003 *J. Appl. Phys.* **93** 3414
[3] Piquer C, Grandjean F, Isnard O, Pop V and Long G J 2004 *J. Appl. Phys.* **95** 6308
[4] Piquer C, Isnard O, Grandjean F and Long G J 2003 *J. Magn. Magn. Mater.* **263** 235–242
[5] Piquer C, Isnard O, Grandjean F and Long G J 2003 *J. Magn. Magn. Mater.* **265** 156
[6] Piquer C, Grandjean F, Long G J and Isnard O 2003 *J. Alloys Compounds* **353** 33–41
[7] Piquer C, Hermann R P, Grandjean F, Isnard O and Long G J 2003 *J. Phys.: Condens. Matter* **15** 7395
[8] Piquer C, Grandjean F, Isnard O, Pop V and Long G J 2004 *J. Alloys Compounds* **277** 1
[9] Piquer C, Grandjean F, Long G J and Isnard O 2005 *J. Alloys Compounds* **388** 6
[10] Piquer C, Grandjean F, Long G J and Isnard O 2006 *J. Phys.: Condens. Matter* **18** 221
[11] Ok H N, Baek K S and Kim C S 1981 *Phys. Rev.* B **24** 6600
[12] Isnard O, Vulliet P, Sanchez J P and Fruchart D 1998 *J. Magn. Magn. Mater.* **189** 47
[13] Long G J, Hautot D, Grandjean F, Morelli D T and Meisner G P 2000 *Phys. Rev.* B **60** 7410
[14] Herber R H 1984 *Chemical Mössbauer Spectroscopy* ed R H Herber (New York: Plenum) p 199

[15] Gelato L 1981 *J. Appl. Crystallogr.* **14** 141
[16] Piquer C, Rubin J, Bartolomé J, Kunzcer V and Filoti G 2005 in preparation
Piquer C 2001 *PhD Thesis* University of Zaragoza
[17] Greenwood N N and Gibb T C 1971 *Mössbauer Spectroscopy* (London: Chapman and Hall)
[18] Thomas M F and Johnson C E 1986 *Mössbauer Spectroscopy* ed D E Dickson and F J Berry (Cambridge: Cambridge University Press) p 143
[19] Niculescu V A, Burch T J and Budnick J I 1983 *J. Magn. Magn. Mater.* **39** 223
[20] Li Z W, Zhou X Z and Morrish A H 1992 *J. Phys.: Condens. Matter* **4** 10409
[21] Coehoorn R, Denissen C J M and Eppenga R 1991 *J. Appl. Phys.* **68** 6222
[22] Beurle T and Fähnle M 1992 *J. Magn. Magn. Mater.* **110** L29
[23] Kawakami M, Hihara T, Koi Y and Wakiyama T 1972 *J. Phys. Soc. Japan* **33** 1591
[24] García L M, Chaboy J, Bartolomé F and Goedkoop J B 2000 *Phys. Rev. Lett.* **85** 429
[25] Chaboy J, Laguna-Marco M A, Sanchez M C, Maruyama H, Kawamura N and Suzuki M 2004 *Phys. Rev.* B **69** 134421
[26] Dunlap B D, Nowik I and Levy P M 1973 *Phys. Rev.* B **7** 4322
[27] Williamson D L 1978 *Mössbauer Isomer Shifts* ed G K Shenoy and F E Wagner (Amsterdam: North-Holland) p 317